Available online at www.sciencedirect.com

ScienceDirect

journal homepage: www.elsevier.com/locate/watres

Batch and column sorption of arsenic onto iron-impregnated biochar synthesized through hydrolysis

Xin Hu [a,c], Zhuhong Ding [b,c], Andrew R. Zimmerman [d], Shengsen Wang [e], Bin Gao [c,*]

[a] State Key Laboratory of Analytical Chemistry for Life Science, Center of Material Analysis and School of Chemistry and Chemical Engineering, 20 Hankou Road, Nanjing University, Nanjing 210093, PR China
[b] School of Environment, Nanjing University of Technology, 30 Puzhu Southern Road, Nanjing 211816, PR China
[c] Department of Agricultural and Biological Engineering, University of Florida, Gainesville, FL 32611, USA
[d] Department of Geological Sciences, University of Florida, Gainesville, FL 32611, USA
[e] Department of Soil and Water Science, University of Florida, Gainesville, FL 32611, USA

ARTICLE INFO

Article history:
Received 15 June 2014
Received in revised form
5 October 2014
Accepted 6 October 2014
Available online 14 October 2014

Keywords:
Low-cost sorbents
Characterization
Adsorption mechanism
Arsenic speciation
Regeneration

ABSTRACT

Iron (Fe)-impregnated biochar, prepared through a novel method that directly hydrolyzes iron salt onto hickory biochar, was investigated for its performance as a low-cost arsenic (As) sorbent. Although iron impregnation decreased the specific surface areas of the biochar, the impregnated biochar showed much better sorption of aqueous As (maximum sorption capacity of 2.16 mg g^{-1}) than the pristine biochar (no/little As sorption capacity). Scanning electron microscope equipped with an energy dispersive spectrometer and X-ray diffraction analysis indicated the presence of crystalline Fe hydroxide in the impregnated biochar but no crystal forms of arsenic were found in the post-sorption biochar samples. However, large shifts in the binding energy of Fe_{2p}, As_{3d}, O_{1s} and C_{1s} region on the following As sorption indicated a change in chemical speciation from As(V) to As(III) and Fe(II) to Fe(III) and strong As interaction with oxygen-containing function groups of the Fe-impregnated biochar. These findings suggest that the As sorption on the Fe-impregnated biochar is mainly controlled by the chemisorption mechanism. Columns packed with Fe-impregnated biochar showed good As retention, and was regenerated with 0.05 mol L^{-1} $NaHCO_3$ solution. These findings indicate that Fe-impregnated biochar can be used as a low-cost filter material to remove arsenic from aqueous solutions.

1. Introduction

Arsenic is one of the most common environmental pollutants throughout the world (Bhattacharya et al., 2007). It has been confirmed that arsenic compounds have detrimental effects on human health (Jomova et al., 2011; Basu et al., 2014) and has been recognized as group 1 carcinogens by the International Agency for Research on Cancer (IARC) (Jomova et al., 2011).

* *Corresponding author*. Tel.: +1 352 392 1864x285; fax: +1 352 392 4092.
E-mail address: bg55@ufl.edu (B. Gao).
http://dx.doi.org/10.1016/j.watres.2014.10.009
0043-1354/

A maximum arsenic concentration of 10 μg/L in drinking water has recommended by World Health Organization (WHO) in 1993 (Khan and Ho, 2011). Inorganic arsenic in water and wastewater may result from the weathering of arsenic-containing minerals and ores and from industrial discharge (Mudhoo et al., 2011). Inorganic arsenic has high solubility and mobility in acidic, neutral and alkaline water and the most common species of inorganic arsenic in water and wastewater at neutral pH are arsenate [$H_2AsO_4^-$, As(V)] and arsenite [H_3AsO_3, As(III)] (Bhattacharya et al., 2007; Mudhoo et al., 2011). Because arsenic contamination in groundwater affects millions of people globally (Brammer and Ravenscroft, 2009; Akter and Ali, 2011) methods to remove arsenic from drinking water and wastewater are urgently required.

Arsenic removal methods include precipitation, lime softening, membrane separation, ion exchange but sorption is one of the most commonly used removal methods due to its ease of operation, relatively low cost, and no sludge disposal (Mohan and Pittman, 2007). Various types of sorbents have been developed and applied for water treatment during the past few decades (Yadanaparthi et al., 2009). Among them, iron oxyhydroxide powders are considered to be one of the most efficient sorbents for arsenic in aqueous solutions (Saharan et al., 2014). However, separation of spent iron oxyhydroxides particles requires sedimentation or filtration, which results in additional cost and low mechanical resistance (Tuna et al., 2013). Activated carbon (AC) is another sorbent that has been widely used to remove water pollutants because of its high specific surface area, abundant surface functional groups, and well-developed pore structures. However, AC is not suitable for removing some anionic contaminants such as arsenic because most likely its surface is negative charged (Cooper et al., 2010; Yao et al., 2011). Composite sorbents that combine AC and iron oxyhydroxides (i.e., iron-loaded AC) thus have been developed to solve the problems and the composites can effectively remove arsenic from aqueous solutions (Chang et al., 2010; Nieto-Delgado and Rangel-Mendez, 2012). Despite that, arsenic removal by iron-loaded AC is still not a cost-effective process because the production of AC itself is expensive and may not necessarily be environmentally 'friendly' (Hjaila et al., 2013). Alternative and low-cost sorbents thus are still needed for the removal of arsenic from aqueous solutions.

Biochar is another carbonaceous material that can be obtained from pyrolysis of agricultural waste and by-products and has been used in many environmental applications (Zimmerman et al., 2011; Ahmad et al., 2014). Because of its relatively low cost and widespread availability, biochar has also been suggested to be an alternative adsorbent for wastewater treatment (Mohan et al., 2014). In the literature, however, only few studies have examined the sorption of arsenic on biochar or biochar-based sorbents (Zhang and Gao, 2013; Zhang et al., 2013; Mohan et al., 2014). In a previous study, Zhang et al. (2013) found that biochar loaded with Fe_2O_3 particles can be prepared directly from $FeCl_3$ treated biomass through pyrolysis and the iron-loaded biochar shows excellent sorption ability to arsenic in water. Because the feedstock needs to be treated with superabundant of iron salt (Zhang et al., 2013), the produce of the Fe_2O_3/biochar composites may generate large amount of ashes, which may cause problems in large-scale productions. Additional investigations are still needed to develop easy and innovative synthesis to prepare low-cost, iron-loaded biochars for the removal of arsenic from aqueous solutions. Furthermore, only batch sorption experiments were conducted to examine arsenic removal by biochar in previous studies (Zhang and Gao, 2013; Zhang et al., 2013; Mohan et al., 2014), there is also a need to evaluate the performance of iron-loaded biochar in fixed-bed columns.

In this work, biochar was derived from the hickory chips and then impregnated with iron nanoparticles using a facile method of direct hydrolysis of iron salt. Both batch and fixed-bed column experiments were carried out to examine and compare the sorption characteristics of As(V) onto pristine and iron(Fe)-impregnated biochars. The sorption mechanism of As on the iron-impregnated biochar was further explored using a variety of characterization tools including scanning electron microscope equipped with an energy dispersive spectrometer (SEM-EDS), X-ray diffraction (XRD), thermogravimetric analyzer (TGA), Fourier transform infrared spectra (FTIR) and X-ray photoelectron spectroscopy (XPS). The main objectives of this work were to: 1) develop a simple and easy-to-operate method for preparing low-cost As sorbents; 2) evaluate the As removal ability of the Fe-impregnated biochar; and 3) determine the sorption mechanism of As onto the Fe-impregnated biochar.

2. Materials and methods

2.1. Chemical reagents

All the chemical reagents used were of analytic grade, except as noted and solutions were prepared using deionized (DI) water (18 MΩ·cm). Ferrous nitrate ($Fe(NO_3)_3 \cdot 9H_2O$), sodium arsenate ($Na_2HAsO_4 \cdot 12H_2O$), sodium bicarbonate ($NaHCO_3$) were purchased from Fisher Scientific and hickory chips were collected from local farm.

2.2. Preparation of sorbents

Dried hickory chips was ground in a knife mill (Model No. 4, Arthur H. Thomas Company, Philadelphia, PA) to achieve particle diameters between 0.5 mm and 1 mm. These were then placed inside tubular quartz reactors (50 g in 6 cm diameter × 28 cm cylinders), which were purged with nitrogen gas (10 psi) and placed inside a bench-top furnace (Barnstead 1500 M/Olympic 1823 HE). The furnace was then ramped to 600 °C at a rate of 20 °C/min and held 2 h at that temperature with the above flowing rate of nitrogen gas. The biochar samples produced were washed with tap water and deionized water several times, oven dried (80 °C), and placed in a sealed container prior to use.

Fe-impregnated biochar was prepared through direct hydrolysis of iron salt following the reaction: $Fe(NO_3)_3 + 3H_2O \Rightarrow Fe(OH)_3 + 3HNO_3$. Solutions of iron salt, prepared by dissolving 7.23 g of $Fe(NO_3)_3 \cdot 9H_2O$ in 40 ml of DI water, were mixed with 10 g of biochar for 12 h under continuous strong agitation using a magnetic stirrer, and then dried at 100–120 °C. The dried composites were washed with

de-ionized water several times to remove surface iron hydroxide, then again oven dried (80 °C). The resulting product is the Fe-impregnated biochar.

2.3. Sorbent characterization

Contents of carbon, hydrogen and nitrogen in the samples were determined using a CHN Elemental Analyzer (Carlo–Erba NA–1500). Fe in biochar was determined using inductively coupled plasma optical emission spectroscopy (ICP–OES, Perkin Elmer Optima 2100 DV, USA) after ashing at the temperature of 550 °C and acid dissolution. Specific surface areas of the samples were measured with a Quantachrome Autosorb-1 surface area analyzer using N_2 (BET) sorption methods. The curves of thermogravimetry (TG) and differential scanning calorimetry (DSC) for sorbents were carried out using a Mettler TGA/DSC thermogravimetric analyzer (TGA/DSC 1, STARe System, METTLER TOLEDO, USA) at a heating rate of 10 °C/min from 50 °C to 800 °C in atmosphere. A JEOL JSM-6330F field-emission SEM-EDS was used to examine and compare surface morphology and elemental composition of samples. Crystalline Fe minerals in char samples were detected using an XRD (Philips Electronic Instruments). FTIR spectra of the pristine biochar and the pre- or post-sorption Fe-impregnated biochar samples were recorded in the range 400–4000 cm^{-1} with 2 cm^{-1} resolution using a Nicolet 6700 FTIR (Thermo Scientific) after samples were milled with potassium bromide (KBr) to form a very fine powder and then compressed into a thin pellet for analysis. Composition and speciation of surface elements of biochar samples were analyzed by using XPS with a PHI 5100 series ESCA spectrometer (Perkin Elmer).

2.4. Batch aqueous As sorption

Batch sorption experiments were carried out at room temperature (20 ± 2 °C) by adding 0.1 g sorbent to 100 mL polyethylene centrifuge tubes containing 50 mL As solution of concentrations between 0.1 and 55 mg L^{-1} (i.e., 0.1, 0.5, 2, 5, 10, 25, 55 mg L^{-1}). The solution pH was adjusted to 5.8 ± 0.2 for each experiment using 0.01 mol L^{-1} NaOH or 0.01 mol L^{-1} HCl. After shaking 24 h in a rotary shaker for equilibration sorption, the mixture was centrifuged at 4000 rpm for 10 min. Concentrations of As in the supernatants was determined using inductively coupled plasma optical spectrometry (ICP–OES, Optima 2300, Perkin–Elmer SCIEX, USA). The amounts of sorbed As (q_t) per unit sorbent mass were calculated based as the differences between initial and final aqueous solution concentrations. The residual solids were washed with deionized water and then oven dried (80 °C) and stored for analysis using SEM, XRD, FT-IR, XPS and TG-DSC.

Influence of co-existing anions (5 mg L^{-1} of SO_4^{2-}, NO_3^-, and Cl^-; and 5 and 50 mg L^{-1} of PO_4^{3-}, respectively) on As (5 mg L^{-1}) sorption onto the Fe-impregnated biochar was carried out using the same procedures.

2.5. Column sorption and regeneration

About 1 g of the test biochar was wet-packed as an interlayer in an acrylic column measuring 5 mm in diameter. About 9.4 g of acid-cleaned quartz sand (0.5–0.6 mm average size) was used at each end of the column to help distribute the flow. The final height of the biochar layer was 12 mm. The column was initially flushed with DI water for about 2 h. A peristaltic pump (Masterflex L/S, Cole Parmer Instrument, Vernon Hills, IL) was used at the influent (bottom) of the column to maintain an upward flow rate in the column of 2 mL/min. The column experiment was initiated by switching the influent to a 50 mg L^{-1} As solution (pH = 5.8 ± 0.2) for about 70 min. The column was then flushed with DI water for another 70 min. Column effluent samples were collected every 2 min with a fraction collector (IS-95 Interval Sampler, Spectrum Chromatography, Houston, TX) during the experiment and analyzed for As concentrations. After the DI water flushing, the regeneration experiment was initiated by switching to 0.05 mol L^{-1} $NaHCO_3$ (Anawar et al., 2003) solution at the same flow rate for 60 min.

3. Results and discussion

3.1. Batch sorption of As onto biochars

Batch aqueous sorption experiments showed that little As was adsorbed by the pristine biochar, however, the Fe-impregnated biochar showed much better As adsorption ability (Fig. 1). For both isotherms, adsorption of As increased rapidly with increasing equilibrium As concentration and then reached constant (Fig. 1). Little As was adsorbed onto the pristine biochar, probably because its surface is negatively charged, which may generate electrostatic repulsions to reduce the adsorption of As. Previous studies have suggested that most of the pristine biochars prepared from slow pyrolysis are negatively charged and thus have limited ability to adsorb anions such as arsenate and phosphate (Mukherjee et al., 2011; Yao et al., 2011, 2012).

The Langmuir, Freundlich, and Temkin isotherm models were applied to describe the adsorption of As onto the Fe-impregnated biochar (Fig. 1). The Langmuir isotherm, which assumes monolayer coverage of sorbent over a homogeneous sorbent surface composed of a finite number of identical sites

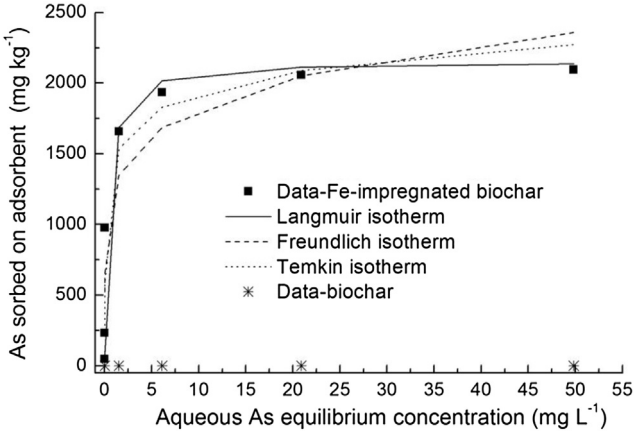

Fig. 1 – Sorption isotherms of As onto pristine and Fe-impregnated biochars.

with equal sorption activation energies (Langmuir, 1916), simulated the data fairly well with the coefficient of determination (R^2) of 0.812. The maximum sorption capacities for As obtained from Langmuir model was 2.16 mg g^{-1} and the Langmuir constant, K_L, which denotes sorption energy, was found to be 2.36 L mg^{-1}. The dimensionless parameter of the equilibrium or sorption intensity (*RL*), calculated using the sorption constant K_L and the initial concentration of As, were all in the range of 0 and 1, suggesting 'favorable' sorption (Weber and Chakravorti, 1974). The isotherms suggest high affinity surface sorption mechanism for As on Fe-impregnated biochar. The Freundlich isotherm, which is often used for describing chemisorption process, fitted the data slightly better ($R^2 = 0.853$) than the Langmuir model (Fig. 1). The best-fit Freundlich constants, K_F and *n*, are 1260 mL^3 g^{-1} and 0.160, respectively. Because the *n* value is below unity, the adsorption of As onto the Fe-impregnated biochar could be affected by chemisorption mechanisms under the tested experimental conditions (Ozcan et al., 2005). In the literature, the Temkin isotherm model is often used to explore the energy distribution of the sorption process (Samarghandi et al., 2009). The Temkin isotherm described the data ($R^2 = 0.935$) better than the other two models (Fig. 1). The constants *A* and b_T obtained for Temkin isotherm model are 210.5 L g^{-1} and 11.7, respectively, further confirming that chemisorption played an important role in controlling the sorption of As onto the Fe-impregnated biochar.

The maximum As(V) sorption capacity of Fe-impregnated biochar was similar to or greater than that of many previously reported Fe-impregnated adsorbents (Table 1). In comparison with other commercial adsorbents such as AC, biochar is relatively low cost and can be obtained from a variety of biomass feedstocks, including waste biomass. Furthermore, the Fe-impregnated biochar developed in this work was synthesized through direct hydrolysis of iron salt, which is much more convenient and cost-effective for large-scale operations than other syntheses of iron-loaded biochars reported in previous studies (Zhang et al., 2013). Taking As sorption capacity and the preparation costs into account, the Fe-impregnated biochar may be an excellent alternative for the efficient treatment of wastewater containing arsenic and warrants further investigation.

Coexisting anions may influence aqueous phase equilibrium during As sorption. Therefore, The effects of main anions (5 mg L^{-1} for SO_4^{2-}, NO_3^- and Cl^- and 5 and 50 mg L^{-1} for PO_4^{3-}, respectively) on As (5 mg L^{-1}) sorption showed that the equilibrium sorption capacities was unaffected by the presence of SO_4^{2-}, NO_3^- and Cl^- (Fig. 2). The presence of PO_4^{3-}, however, dramatically decreased the sorbent's As sorption ability and this effect aggravated with the increasing of PO_4^{3-} concentration (i.e., from 5 to 50 mg L^{-1}) (Fig. 2). This may be attributed to the fact that arsenate and phosphate have similar ionic structures and compete for the same adsorption sites. Competitive sorption of phosphate with arsenate has been reported for various types of adsorbents in the literature (Li et al., 2012; Badruddoza et al., 2013).

3.2. Column sorption and regeneration

The column breakthrough curves for Fe-impregnated biochar, with flow rate of 2 mL/min, shows fast uptake of As in the initial stages and rapid decrease as saturation was reached (Fig. 3a). The convection-dispersion-reaction (CDER) kinetic model was used to analyze the column experimental data. The governing equations are listed as follows (Chen et al., 2011):

$$R\frac{\partial C}{\partial t} + \frac{\rho_b}{\theta}\frac{\partial q}{\partial t} = D\frac{\partial^2 C}{\partial z^2} - v\frac{\partial C}{\partial z} \quad (1)$$

$$\frac{\rho_b}{\theta}\frac{\partial q}{\partial t} = kC \quad (2)$$

where *R* is the retardation factor (dimensionless), *C* is the sorbate concentration in pore water (mg L^{-1}), *t* is time (min), ρ_b

Table 1 – Comparison of max sorption capacity of As(V) by ferruginous sorbents.

Sorbents	Max sorption capacity (mg/g)	Experimental conditions		References
		Initial As(V) concentration (mg/L)	Solution pH	
Iron hydro(oxide) nanoparticles/ activated carbons	0.37–1.25	0–1	6–8	Vitela-Rodriguez and Rangel-Mendez (2013)
Iron hydro(oxide) nanoparticles/ activated carbon	1.65–3.25	0–10	7	Nieto-Delgado and Rangel-Mendez (2012)
Fe-impregnated granular activated carbon	1.95	0–40	7	Chang et al. (2010)
γ-Fe_2O_3 composite/biochar	3.15	0–200	Not reported	Zhang et al. (2013)
Fe (III)-loaded chitosan hollow fibers	3.70	0–0.3	3.5	Dorraji et al. (2014)
Iron oxide hydroxide nanoflower	0.48	0–1	Not reported	Raul et al. (2014)
Fe(III)-coated rice husk.	2.50	0–75	4	Pehlivan et al. (2013)
Iron-oxide-coated natural rock	1.65	0–0.6	5.7 ± 0.2	Maji et al. (2013)
Magnetic iron oxide/multiwall carbon nanotubes	9.74	0–11	5.5	Ma et al. (2013)
Fe(II)-loaded activated carbon	2.20/3.01	0–8.5	3	Tuna et al. (2013)
Bituminous/wood based iron-modified AC	2.28/2.45	0–4	7	Arcibar-Orozco et al. (2014)
Iron-coated honeycomb briquette cinder	0.96	0–0.5	7.5	Sheng et al. (2014)
Iron oxide amended rice husk char	0.95–1.46	0–2.5	6.85 ± 0.23	Cope et al. (2014)
Iron-impregnated biochar	2.16	0–55	5.8 ± 0.2	This study

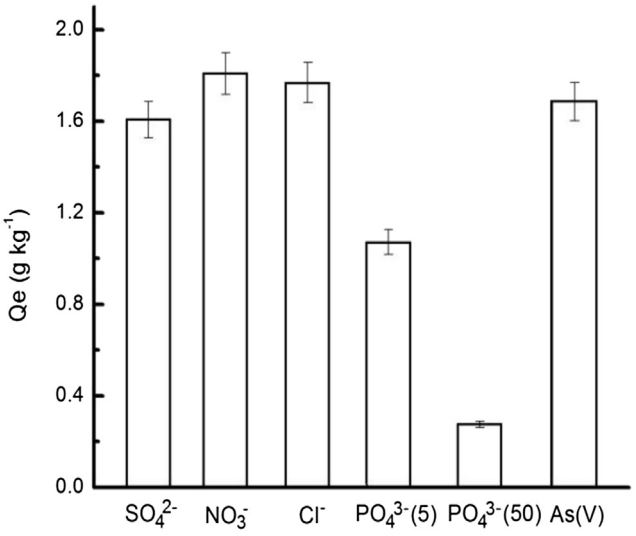

Fig. 2 – Effect of coexisting anions (SO_4^{2-}, NO_3^- and Cl^{-1}: 5 mg L^{-1}; PO_4^{3-}: 5 and 50 mg L^{-1}) on As (5 mg L^{-1} initial concentration) sorption onto Fe-impregnated biochar.

is the medium bulk density (g L^{-1}), θ is the dimensionless volumetric moisture content, q is the quantity of sorbed As (mg g^{-1}), z is the distance traveled in the direction of flow (cm), D is the dispersion coefficient (cm^2 min^{-1}), v is the average linear pore-water velocity (cm min^{-1}), and k is the first-order removal rate constant (min^{-1}). Equations (1) and (2) were solved numerically with a zero initial concentration, a pulse-input and a zero-concentration-gradient boundary conditions for the whole column. The Levenberg–Marquardt algorithm was used to estimate the value of the model parameters by minimizing the sum-of-the-squared differences between model-calculated and measured effluent concentrations over multiple calculation iterations. The breakthrough curve data for the sorption column was well fitted by the CDER model ($R^2 = 0.990$) (Fig. 3). The obtained best-fit R and k values were 20 and 0.06 min^{-1}, respectively, indicating that the Fe-impregnated biochar had strong As sorption ability and can be used as an effective sorption media in filters and reactive barriers to remove As from flowing water.

Regeneration ability of a sorbent is a desirable quality to enable the recycling of both the sorbate and sorbent. A 0.05 mol L^{-1} $NaHCO_3$ solution was found to efficiently regenerate the column by desorbing As from the Fe-impregnated biochar (Fig. 3b). Concentrations of As in column effluent reached a low of 1.63 mg L^{-1} after 60 min of leaching (Fig. 3b). Mass balance calculations showed that, of the 830 μg of As initially retained in the column, 85% (710 μg) were flushed out after the regeneration with $NaHCO_3$. Other alkaline regeneration agents, such as NaH_2PO_4, have also been used previously in As desorption (Tuutijarvi et al., 2012; Gao et al., 2013), and should be tested in the future to optimize of the regeneration of Fe-impregnated biochar columns for As removal.

3.3. *Physicochemical properties and sorption mechanism*

The Fe contents of biochar and Fe-impregnated biochar were 0.03% and 3.88%, respectively, suggesting that iron was successfully impregnated into biochar. The C, N and H contents of biochar were 84.7, 0.30 and 1.73%, respectively, and 68.8%, 1.83 and 2.03% for Fe-impregnated biochar, respectively. Specific surface areas were 256 m^2 g^{-1} biochar and 16.0 m^2 g^{-1} for Fe-impregnated biochar, respectively, suggesting that iron impregnation filled pores or clogged pore-openings on biochar surfaces. Thus, specific surface areas cannot be considered the key parameter in determining As sorption onto biochar. The morphology of the obtained sorbents was observed using SEM under different magnifications and mainly showed no regular or amorphous characteristics (Fig. 4). Those may be result from the grinding during sample preparation. While, EDS showed the occurrence of Fe on the surface of the Fe-impregnated biochar, no As was found on the post-sorption biochars, which might be because the content of As adsorbed on the Fe-impregnated biochar was below the determination limit of EDS (Fig. 4).

Carbon in biochar existed mainly in the amorphous forms while quartz and calcite were present in the pristine biochar (Fig. 5). Instead of these minerals, goethite was found in Fe-impregnated biochar both before and after As sorption

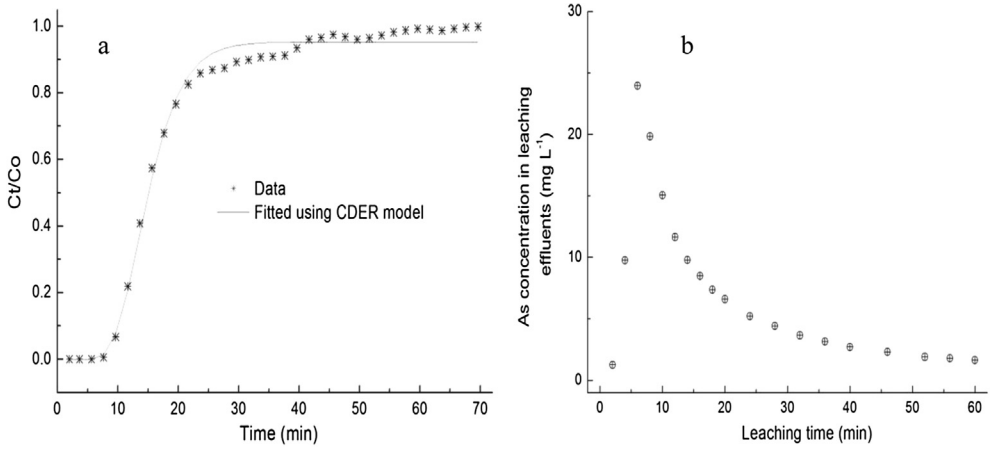

Fig. 3 – As filtration in fixed-bed column packed with Fe-impregnated biochar: (a) As breakthrough curve, and (b) As desorption using 0.05 mol L^{-1} $NaHCO_3$.

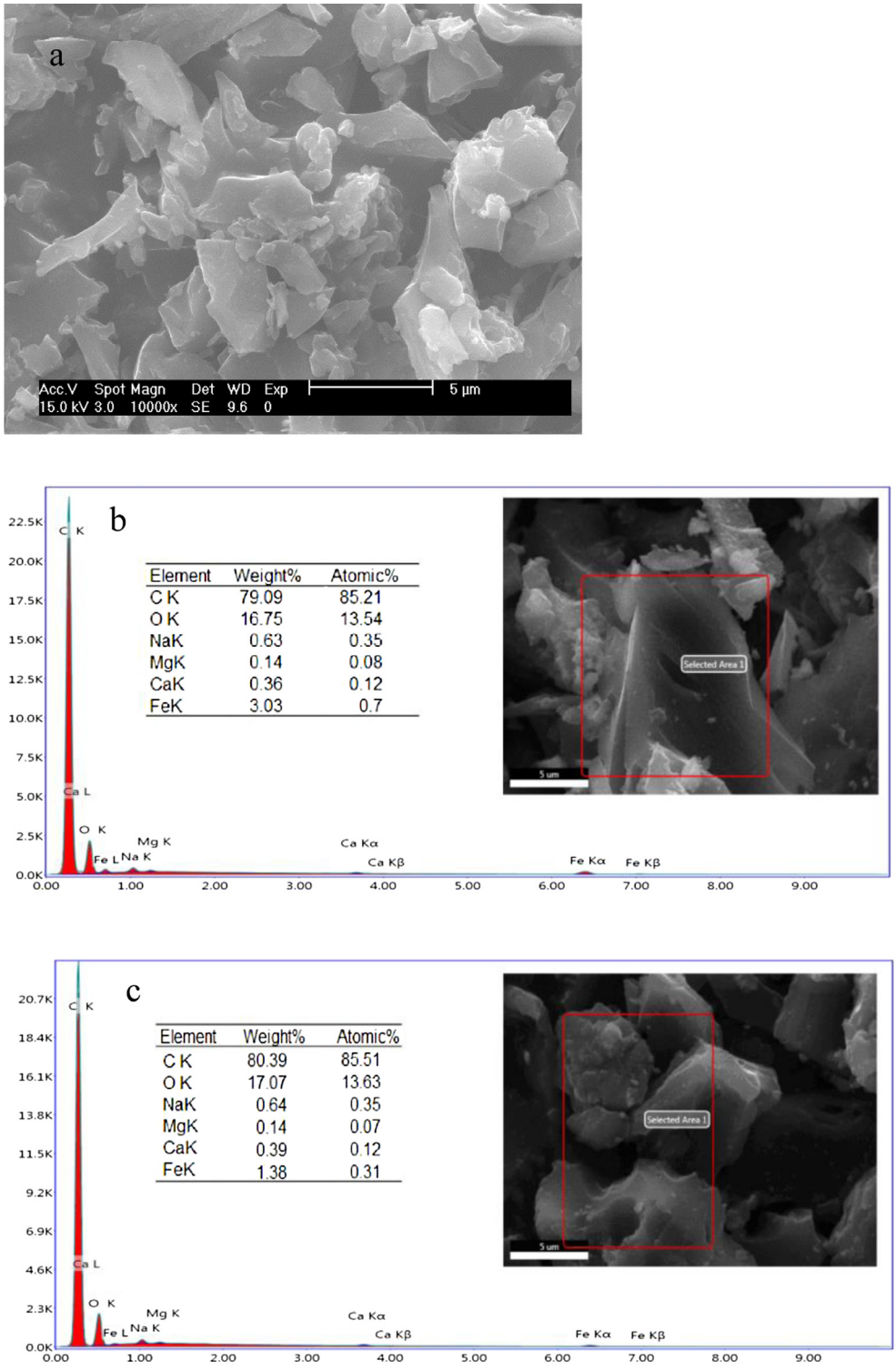

Fig. 4 – SEM-EDS analysis of (a) pre-sorption Fe-impregnated biochar (b) and post-sorption Fe-impregnated biochar.

(Fig. 5). No crystal forms of adsorbed As was found, suggesting that As only reacted with the goethite's surface and sorption did not change its crystal structure or form a separate precipitate phase (Fig. 5).

Thermal decomposition resulted in the greatest mass loss in the temperature range of about 350–600 °C for biochar, which differed greatly with Fe-impregnated biochar and the Fe-impregnated biochar adsorbed As (Fig. 6). The masses remaining, compared to the initial mass, were 4.55% for biochar, 9.51% for Fe-impregnated biochar, and 11.0% for Fe-impregnated biochar with sorbed As. The combustible components in biochars react with oxygen to product CO_2 and H_2O

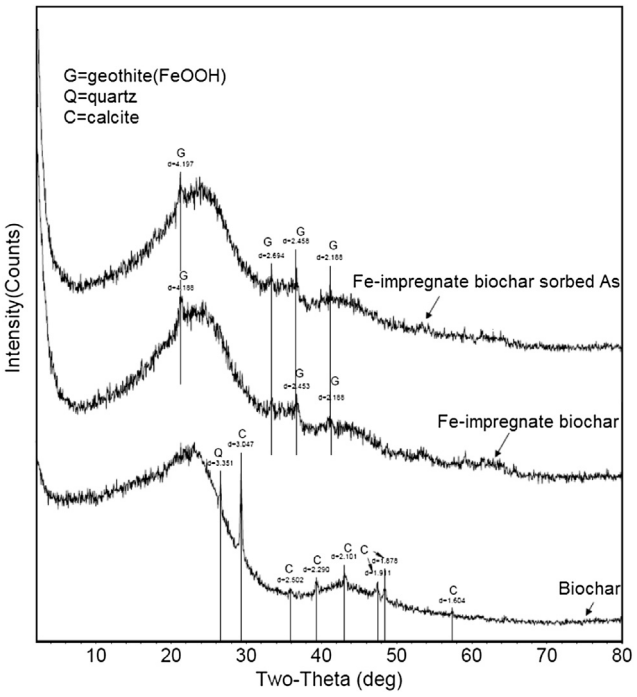

Fig. 5 – XRD patterns of post-sorption Fe-impregnated biochar (uppermost), pre-sorption Fe-impregnated biochar (middle), and pristine biochar (lowermost).

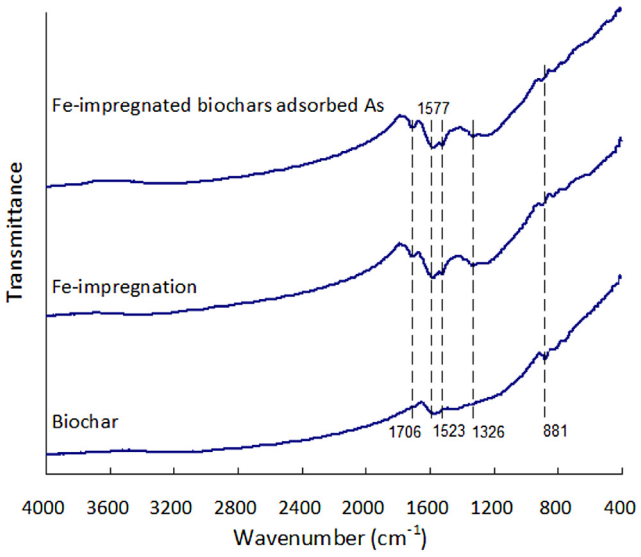

Fig. 7 – FTIR spectra of pristine biochar and pre- and post-sorption Fe-impregnated biochar samples.

and the burning point is in the order of Fe-impregnated biochar < Fe-impregnated biochar adsorbed As < biochar from the DTG curve (Fig. 6). The DTG curve in Fig. 6 shows that the main peak values were about 0.80%/°C for biochar, 0.89%/°C for Fe-impregnated biochar, 0.58%/°C for Fe-impregnated biochar adsorbed As, respectively and the corresponding temperature were about 352 °C for biochar, 336 °C for Fe-impregnated biochar, 354 °C for Fe-impregnated biochar adsorbed As, respectively. Those suggested the different inflammability of those biochars. The DSC curves of the combustion process in Fig. 6 represent the variations of the combustion heat release rate with the increasing temperature, suggesting the different exothermic properties for those biochars. The Fe-impregnation and sorption process change the exothermic properties of biochars (Fig. 6).

The differences of FT-IR spectra of the studied biochar samples were mainly focused on the wavenumber interval of 1800–800 cm^{-1}. New peaks of FT-IR spectra for the pre- and post-sorption Fe-impregnated biochar samples appear at 1706 and 1523 cm^{-1} (Fig. 7). A peak at 1326 cm^{-1} appeared after Fe impregnation, but weakened greatly after the As sorption

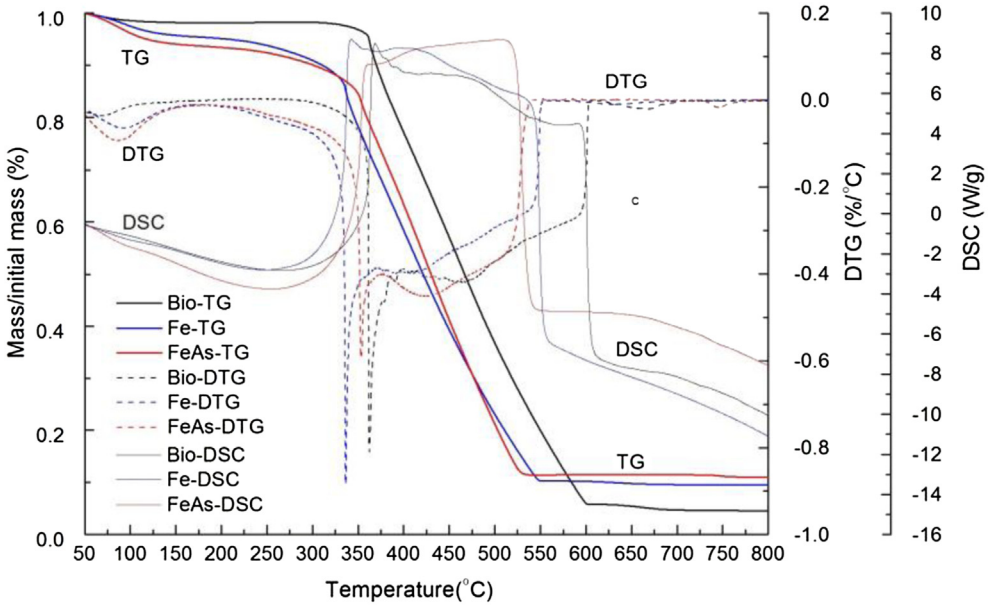

Fig. 6 – TG-DTG and DSC curves of the sorbents (Bio: pristine biochar; Fe: pre-sorption Fe-impregnated biochar; and FeAs: post-sorption Fe-impregnated biochar).

(Fig. 7). It was reported that the characteristic absorption bands of sorbed arsenate was 650–950 cm^{-1} for the As–O stretching vibration (Lumsdon et al., 1984; Jia et al., 2007). A peak at 881 cm^{-1} weakened greatly and blue shifts occurred after the Fe impregnation and the As sorption (Fig. 7), confirming that iron played an important role in As sorption. The C=O stretching peak around 1577 cm^{-1} was similar among the pristine biochar and the pre- and post-sorption Fe-impregnated biochars. Therefore, both Fe impregnation and the As sorption altered the surface functional groups of the biochar.

In order to further investigate the mechanism of arsenic sorption on the Fe-impregnated biochars, binding energy shifts for carbon, oxygen, iron and arsenic were examined using XPS (Fig. 8). Surface of biochar was enriched with only carbon and oxygen while Fe and As appear in biochars after impregnation and sorption, respectively (Fig. 8). Seven prominent iron peaks corresponding to Fe_{3p}, Fe_{3s}, Fe_{2p1}, Fe_{2p3}, Fe LMM, Fe LMM1 and Fe LMM2 were found in the surface of Fe-impregnated biochar both before and after As interaction. Prominent peaks corresponding to As_{3p}, As_{3s}, As_{2p1}, As_{2p3}, As LMM and As LMM1 were observed in the surface of Fe-impregnated biochar adsorbed As. Fig. 8 shows that the atomic percentage of C decreased greatly while that of O increased greatly after iron impregnation. The atomic percentage of Fe and O decreased while that of C increased after As sorption (Fig. 8). The atomic ratios of O/C were 0.14, 0.43 and 0.36 for the pristine biochar and the pre- and post-sorption Fe-impregnated biochars, respectively, suggesting that the oxygen-contained functional groups increased after iron impregnation and decreased after As sorption (Fig. 8).

High-resolution XPS spectra of post-sorption Fe-impregnated biochar in the As_{3d} region showed a single peak at the binding energy of 44.68 eV (Fig. 9a). It is reported that 3d binding energy was 45.5 eV for As(V) in Na_2HAsO_4, 44.2 eV for As(III) in $NaAsO_2$ and 41.5 eV for As(0), respectively (Roberts et al., 1975; Wagner et al., 1979). Some shifts in binding energies of As_{3d} can occur in different arsenic species, for example 44.9 eV for AsO_4^{3-}, 45.5 eV for $HAsO_4^{2-}$, and 46.7 eV for $H_2AsO_4^-$ (Bang et al., 2005). Therefore, 44.68 eV of As_{3d} binding energy in the surface of Fe-impregnated biochar indicates that the As(V) in the initial solution was likely converted partly into As(III) on the surface of the Fe-impregnated biochars during the sorption process. Similarly, a reduction of As(V) to As(III) was reported by Deliyanni et al. (2013) and by Mohan and Pittman (2007) and the reduction of As(III) to As(0) when sorbed on zero-valent iron (Bang et al., 2005).

High-resolution XPS spectra of Fe-impregnated biochar showed double peak at the binding energy of around 710 and 724 eV in the Fe_{2p} region (Fig. 9b), which is similar to that reported by Wu et al. (2012) for Fe_3O_4 nanoparticles on graphene oxide surfaces (Wu et al., 2012). The binding energy of 709 eV and 711 eV of $2p^{3/2}$ can be associated with Fe^{2+} and Fe^{3+}, respectively (Li et al., 2011). The binding energy of 710.09 eV (FeOOH and/or FeO) and 710.66 eV (FeOOH and/or Fe_2O_3) of $2p^{3/2}$ indicates that both Fe^{2+} and Fe^{3+} should be existed. The shifts of 710.09 eV–710.66 eV indicate the oxidation of Fe^{2+} to Fe^{3+} during the sorption process. The oxidation of Fe^{2+} to Fe^{3+}

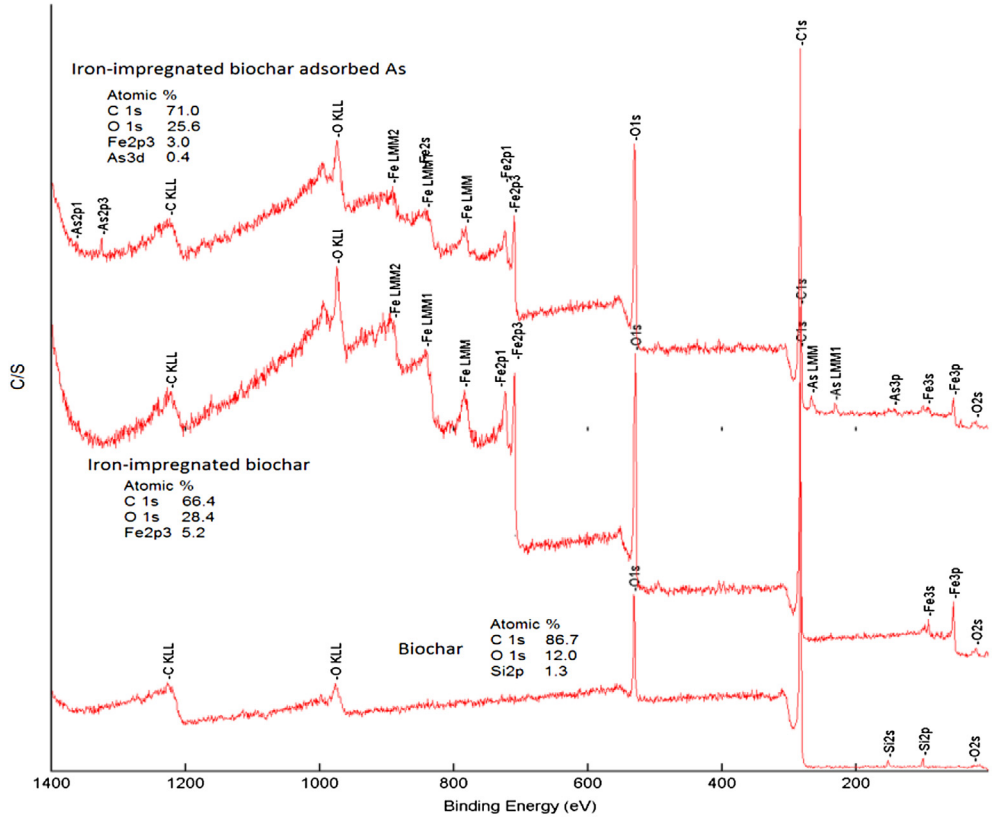

Fig. 8 – XPS analysis of pristine biochar and the pre- and post-sorption Fe-impregnated biochar.

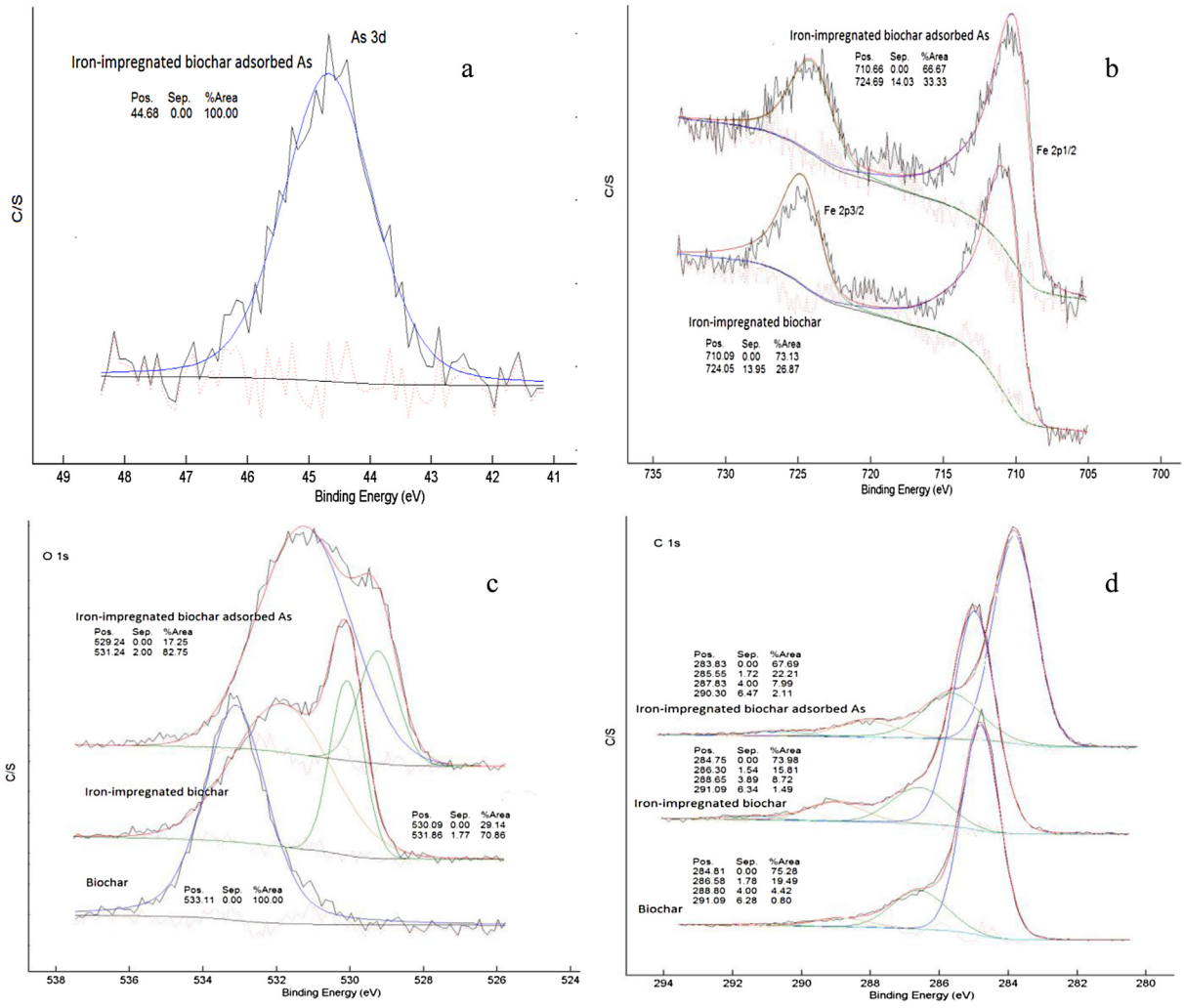

Fig. 9 – XPS analysis of C, O, Fe and As in pristine biochar and pre- and post-sorption Fe-impregnated biochar (a, b, c and d: detail scan of As_{3d}, Fe_{2p}, O_{1s} and C_{1s}).

during the sorption process may have been coupled to the reduction of As(V) to As(III).

O_{1s} peaks are broad, thus indicating the presence of different chemical states of oxygen such as organic oxygen (O in carboxyl, carbonyl, alcoxyl or ether groups) and inorganic oxygen (O in iron oxides) in biochars and Fe-impregnated biochars (Datsyuk et al., 2008). Only one peak appears at the binding energy of 533.11 eV in biochars (Fig. 9c), which can be ascribed to C–OH or O–C. The large shifts were obvious on the binding energy O_{1s} region of the Fe-impregnated biochars and the Fe-impregnated biochars adsorbed As (Fig. 9c). The binding energy in the O_{1s} region between 529.24 eV and 530.09 eV may be attributed to inorganic oxygen bonded to iron (FeO, Fe_2O_3 or FeOOH), corresponding to the results of XRD analysis. There is considerable weakening of peaks at 529.24 eV, which may be due to the sorption of arsenic onto FeOOH phases. The newly appearing peak at the binding energy of 531.24 eV can be attributed to oxygen bonded to As while the peak at the binding energy of 531.86 eV (C=O/O–C=O bonds) disappeared (Fig. 9c). All of this suggests the binding of As and O during the As adsorption, which is consistent with the results of high-resolution XPS spectra in the As_{3d} region.

The binding energy of C_{1s} at 283.83 eV was assigned to C–H, at 284.8 eV to graphite C, at 286.5 ± 0.2 eV to C–O, at 287.8 eV to C=O, at 288.7 eV to C=O/O–C=O and at 290.30 eV to carbonates (Datsyuk et al., 2008). The peak at 285.55 eV can be attributed to C–O single bond (Barinov et al., 2009) while 291.09 eV means the p–p* transitions (Datsyuk et al., 2008). The main peaks at the pristine biochars and Fe-impregnated biochars were similar and differed greatly with them for the Fe-impregnated biochars adsorbed As (Fig. 9d). Therefore, amorphous C and/or Graphite C were the dominant speciation of C in the pristine biochars and Fe-impregnated biochars. Compared with the pristine biochar, Fe impregnation increases the percentage of 288.65 eV, suggesting the increasing of C=O/O–C=O, which may be due to the oxidation of HNO_3 during the hydrolysis of $Fe(NO_3)_3$. After the sorption of As, new dominant peaks appeared at the binding energy of 283.83 eV

(C–H) and 285.55 eV (C–O), indicating significant changes in the surface carbon functional groups of Fe-impregnated biochar.

4. Conclusions

As the first of its kind, this work developed a facile and easy-operation method to produce Fe-impregnated biochar through direct hydrolysis of iron salt. Findings from batch sorption experiments suggested that the Fe-impregnated biochar had strong sorption ability to aqueous As (Langmuir maximum sorption capacity of 2.16 mg g^{-1}). Most of the co-existing anions, except PO_4^{3-}, showed no effects on As removal by the Fe-impregnated biochar. In addition, fixed-bed columns packed with Fe-impregnated biochar also showed excellent As removal ability and a 0.05 mol L^{-1} $NaHCO_3$ solution effectively released about 85% of the retained As in the columns. SEM-EDS, XRD, FTIR, and XPS analyses suggested that iron hydroxide particles on the carbon surface of the biochar played an important role in As sorption and the sorption process was mainly controlled by the chemisorption mechanism. Because this novel synthesis is convenient for large-scale production, the Fe-impregnated biochars developed in this work has great potential for use as a low-cost sorbent material to remove arsenic from water.

Acknowledgment

This work was partially supported by the Natural Science Foundation of Jiangsu Province (BK20131268) and the NSF (CBET-1054405).

REFERENCES

Ahmad, M., Rajapaksha, A.U., Lim, J.E., Zhang, M., Bolan, N., Mohan, D., Vithanage, M., Lee, S.S., Ok, Y.S., 2014. Biochar as a sorbent for contaminant management in soil and water: a review. Chemosphere 99, 19–33.

Akter, A., Ali, M.H., 2011. Arsenic contamination in groundwater and its proposed remedial measures. Int. J. Environ. Sci. Technol. 8 (2), 433–443.

Anawar, H.M., Akai, J., Komaki, K., Terao, H., Yoshioka, T., Ishizuka, T., Safiullah, S., Kato, K., 2003. Geochemical occurrence of arsenic in groundwater of Bangladesh: sources and mobilization processes. J. of Geochem. Explor. 77 (2–3), 109–131.

Arcibar-Orozco, J.A., Josue, D.B., Rios-Hurtado, J.C., Rangel-Mendez, J.R., 2014. Influence of iron content, surface area and charge distribution in the arsenic removal by activated carbons. Chem. Eng. J. 249, 201–209.

Badruddoza, A.Z.M., Shawon, Z.B., Rahman, M.T., Hao, K.W., Hidajat, K., Uddin, M.S., 2013. Ionically modified magnetic nanomaterials for arsenic and chromium removal from water. Chem. Eng. J. 225, 607–615.

Bang, S., Johnson, M.D., Korfiatis, G.P., Meng, X.G., 2005. Chemical reactions between arsenic and zero-valent iron in water. Water Res. 39 (5), 763–770.

Barinov, A., Gregoratti, L., Dudin, P., Rosa, S.L., Kiskinova, M., 2009. Imaging and spectroscopy of multiwalled carbon nanotubes during oxidation: defects and oxygen bonding. Adv. Mater. 21, 1916–1920.

Basu, A., Saha, D., Saha, R., Ghosh, T., Saha, B., 2014. A review on sources, toxicity and remediation technologies for removing arsenic from drinking water. Res. Chem. Intermed. 40 (2), 447–485.

Bhattacharya, P., Welch, A.H., Stollenwerk, K.G., McLaughlin, M.J., Bundschuh, J., Panaullah, G., 2007. Arsenic in the environment: biology and chemistry. Sci. of Total Environ. 379 (2–3), 109–120.

Brammer, H., Ravenscroft, P., 2009. Arsenic in groundwater: a threat to sustainable agriculture in South and South-east Asia. Environ. Int. 35 (3), 647–654.

Chang, Q.G., Lin, W., Ying, W.C., 2010. Preparation of iron-impregnated granular activated carbon for arsenic removal from drinking water. J. of Hazard. Mater. 184 (1–3), 515–522.

Chen, H., Gao, B., Li, H., Ma, L.Q., 2011. Effects of pH and ionic strength on sulfamethoxazole and ciprofloxacin transport in saturated porous media. J. of Contam. Hydrol. 126 (1–2), 29–36.

Cooper, A.M., Hristovski, K.D., Moller, T., Westerhoff, P., Sylvester, P., 2010. The effect of carbon type on arsenic and trichloroethylene removal capabilities of iron (hydr)oxide nanoparticle-impregnated granulated activated carbons. J. of Hazard. Mater. 183 (1–3), 381–388.

Cope, C.O., Webster, D.S., Sabatini, D.A., 2014. Arsenate adsorption onto iron oxide amended rice husk char. Sci. Total Environ. 488, 558–565.

Datsyuk, V., Kalyva, M., Papagelis, K., Parthenios, J., Tasis, D., Siokou, A., Kallitsis, I., Galiotis, C., 2008. Chemical oxidation of multiwalled carbon nanotubes. Carbon 46 (6), 833–840.

Deliyanni, E., Bandosz, T.J., Matis, K.A., 2013. Impregnation of activated carbon by iron oxyhydroxide and its effect on arsenate removal. J. of Chem. Technol. and Biotechnol. 88 (6), 1058–1066.

Dorraji, M.S.S., Mirmohseni, A., Tasselli, F., Criscuoli, A., Carraro, M., Gross, S., Figoli, A., 2014. Preparation, characterization and application of iron (III)-loaded chitosan hollow fiber membranes as a new bio-based As (V) sorbent. J. Polym. Res. 21 (4), 1–13.

Gao, X.B., Su, C.L., Wang, Y.X., Hu, Q.H., 2013. Mobility of arsenic in aquifer sediments at Datong Basin, northern China: effect of bicarbonate and phosphate. J. of Geochem. Explor. 135, 93–103.

Hjaila, K., Baccar, R., Sarra, M., Gasol, C.M., Blanquez, P., 2013. Environmental impact associated with activated carbon preparation from olive-waste cake via life cycle assessment. J. of Environ. Manag. 130, 242–247.

Jia, Y.F., Xu, L.Y., Wang, X., Demopoulos, G.P., 2007. Infrared spectroscopic and X-ray diffraction characterization of the nature of adsorbed arsenate on ferrihydrite. Geochimica Cosmochim. Acta 71 (7), 1643–1654.

Jomova, K., Jenisova, Z., Feszterova, M., Baros, S., Liska, J., Hudecova, D., Rhodes, C.J., Valko, M., 2011. Arsenic: toxicity, oxidative stress and human disease. J. of Appl. Toxicol. 31 (2), 95–107.

Khan, M.A., Ho, Y.S., 2011. Arsenic in drinking water: a review on toxicological effects, mechanism of accumulation and remediation. Asian J. of Chem. 23 (5), 1889–1901.

Langmuir, I., 1916. The constitution and fundamental properties of solids and liquids Part I Solids. J. of Am. Chem. Soc. 38, 2221–2295.

Li, P., Jiang, E.Y., Bai, H.L., 2011. Fabrication of ultrathin epitaxial γ-Fe_2O_3 films by reactive sputtering. J. Phys. D: Appl. Phys. 44 (7), 075003.

Li, R.H., Li, Q., Gao, S., Shang, J.K., 2012. Exceptional arsenic adsorption performance of hydrous cerium oxide

nanoparticles: Part A. Adsorption capacity and mechanism. Chem. Eng. J. 185, 127–135.
Lumsdon, D.G., Fraser, A.R., Russell, J.D., Livesey, N.T., 1984. New infrared band assignments for the arsenate ion adsorbed on synthetic goethite (Alpha-Feooh). J. Soil Sci. 35 (3), 381–386.
Ma, J., Zhu, Z.L., Chen, B., Yang, M.X., Zhou, H.M., Li, C., Yu, F., Chen, J.H., 2013. One-pot, large-scale synthesis of magnetic activated carbon nanotubes and their applications for arsenic removal. J. Mater. Chem. A 1 (15), 4662–4666.
Maji, S.K., Kao, Y.H., Liao, P.Y., Lin, Y.J., Liu, C.W., 2013. Implementation of the adsorbent iron-oxide-coated natural rock (IOCNR) on synthetic As(III) and on real arsenic-bearing sample with filter. Appl. Surf. Sci. 284, 40–48.
Mohan, D., Pittman, C.U., 2007. Arsenic removal from water/wastewater using adsorbents – a critical review. J. of Hazard. Mater. 142 (1–2), 1–53.
Mohan, D., Sarswat, A., Ok, Y.S., Pittman, C.U., 2014. Organic and inorganic contaminants removal from water with biochar, a renewable, low cost and sustainable adsorbent – a critical review. Bioresour. Technol. 160, 191–202.
Mudhoo, A., Sharma, S.K., Garg, V.K., Tseng, C.H., 2011. Arsenic: an overview of applications, health, and environmental concerns and removal processes. Crit. Rev. Environ. Sci. Technol. 41 (5), 435–519.
Mukherjee, A., Zimmerman, A.R., Harris, W., 2011. Surface chemistry variations among a series of laboratory-produced biochars. Geoderma 163 (3–4), 247–255.
Nieto-Delgado, C., Rangel-Mendez, J.R., 2012. Anchorage of iron hydro(oxide) nanoparticles onto activated carbon to remove As(V) from water. Water Res. 46 (9), 2973–2982.
Ozcan, A.S., Erdem, B., Ozcan, A., 2005. Adsorption of Acid Blue 193 from aqueous solutions onto BTMA-bentonite. Colloids Surf. A-physicochemical Eng. Aspects 266 (1–3), 73–81.
Pehlivan, E., Tran, T.H., Ouedraogo, W.K.I., Schmidt, C., Zachmann, D., Bahadir, M., 2013. Removal of As(V) from aqueous solutions by iron coated rice husk. Fuel Process. Technol. 106, 511–517.
Raul, P.K., Devi, R.R., Umlong, I.M., Thakur, A.J., Banerjee, S., Veer, V., 2014. Iron oxide hydroxide nanoflower assisted removal of arsenic from water. Mater. Res. Bull. 49, 360–368.
Roberts, E.D., Weightman, P., Johnson, C.E., 1975. Photoelectron and $L_{2,3}$ MM Auger-electron energies for arsenic. J. Phys. C-Solid State Phys. 8 (8), 1301–1309.
Saharan, P., Chaudhary, G.R., Mehta, S.K., Umar, A., 2014. Removal of water contaminants by iron oxide nanomaterials. J. Nanosci. Nanotechnol. 14 (1), 627–643.
Samarghandi, M.R., Hadi, M., Moayedi, S., Askari, F.B., 2009. Two-parameter isotherms of methyl orange sorption by pinecone derived activated carbon. Iran. J. Environ. Health Sci. Eng. 6 (4), 285–294.
Sheng, T.T., Baig, S.A., Hu, Y.J., Xue, X.Q., Xu, X.H., 2014. Development, characterization and evaluation of iron-coated honeycomb briquette cinders for the removal of As(V) from aqueous solutions. Arabian J. Chem. 7 (1), 27–36.
Tuna, A.O.A., Ozdemir, E., Simsek, E.B., Beker, U., 2013. Removal of As(V) from aqueous solution by activated carbon-based hybrid adsorbents: Impact of experimental conditions. Chem. Eng. J. 223, 116–128.
Tuutijarvi, T., Vahala, R., Sillanpaa, M., Chen, G., 2012. Maghemite nanoparticles for As(V) removal: desorption characteristics and adsorbent recovery. Environ. Technol. 33 (16), 1927–1936.
Vitela-Rodriguez, A.V., Rangel-Mendez, J.R., 2013. Arsenic removal by modified activated carbons with iron hydro(oxide) nanoparticles. J. Environ. Manag. 114, 225–231.
Wagner, C.D., Riggs, W.M., Davis, L.E., Moulder, J.F., Muilenberg, G.E., 1979. Handbook of X-ray Photoelectron Spectroscopy. Perkin-Elmer Corporation, Physical Electronics Division, Eden Prairie, MN.
Weber, T.W., Chakravorti, R.K., 1974. Pore and solid diffusion models for fixed-bed adsorbers. Aiche J. 20 (2), 228–238.
Wu, H.X., Gao, G., Zhou, X.J., Zhang, Y., Guo, S.W., 2012. Control on the formation of Fe_3O_4 nanoparticles on chemically reduced graphene oxide surfaces. Crystengcomm 14 (2), 499–504.
Yadanaparthi, S.K.R., Graybill, D., von Wandruszka, R., 2009. Adsorbents for the removal of arsenic, cadmium, and lead from contaminated waters. J. of Hazard. Mater. 171 (1–3), 1–15.
Yao, Y., Gao, B., Inyang, M., Zimmerman, A.R., Cao, X.D., Pullammanappallil, P., Yang, L.Y., 2011. Removal of phosphate from aqueous solution by biochar derived from anaerobically digested sugar beet tailings. J. of Hazard. Mater. 190 (1–3), 501–507.
Yao, Y., Gao, B., Zhang, M., Inyang, M., Zimmerman, A.R., 2012. Effect of biochar amendment on sorption and leaching of nitrate, ammonium, and phosphate in a sandy soil. Chemosphere 89 (11), 1467–1471.
Zhang, M., Gao, B., 2013. Removal of arsenic, methylene blue, and phosphate by biochar/AlOOH nanocomposite. Chem. Eng. J. 226, 286–292.
Zhang, M., Gao, B., Varnoosfaderani, S., Hebard, A., Yao, Y., Inyang, M., 2013. Preparation and characterization of a novel magnetic biochar for arsenic removal. Bioresour. Technol. 130, 457–462.
Zimmerman, A.R., Gao, B., Ahn, M.Y., 2011. Positive and negative carbon mineralization priming effects among a variety of biochar-amended soils. Soil Biol. Biochem. 43 (6), 1169–1179.